Nickel-nanodiamond coatings electrodeposited from tartrate electrolyte at ambient temperature

Makarova Irina, Dobryden Illia, Kharitonov Dmitry, Kasach Aliaksandr, Ryl Jacek, Repo Eveliina, Vuorinen Esa

DOI: 10.1016/j.surfcoat.2019.125063

Please cite the publication as follows:

Makarova, I., Dobryden, I., Kharitonov, D., Kasach, A., Ryl, J., Repo, E., Vuorinen, E. (2019). Nickel-nanodiamond coatings electrodeposited from tartrate electrolyte at ambient temperature. Surface and Coatings Technology, vol. 380. DOI: 10.1016/j.surfcoat.2019.125063

Nickel-nanodiamond coatings electrodeposited from tartrate electrolyte at ambient temperature

Irina Makarova [a, b,*], *Illia Dobryden* [c], *Dmitry Kharitonov* [a, d], *Aliaksandr Kasach* [a], *Jacek Ryl* [e], *Eveliina Repo* [b] *and Esa Vuorinen* [f]

[a] *Chemical Technology and Engineering Faculty, Department of Chemistry, Technology of Electrochemical Production and Electronic Engineering Materials, Belarusian State Technological University, Sverdlova str. 13a, 220006, Minsk, Republic of Belarus*

[b] *Department of Separation and Purification, School of Engineering Science, Lappeenranta University of Technology, Skinnarilankatu 34, FI-53850, Finland*

[c] *KTH Royal Institute of Technology, Surface and Corrosion Science Division, School of Engineering Sciences in Chemistry, Biotechnology and Health (CBH), Drottning Kristinas väg 51, SE-100 44 Stockholm, Sweden*

[d] *Jerzy Haber Institute of Catalysis and Surface Chemistry of Polish Academy of Sciences, 30-239, Niezapominajek 8, Krakow, Poland*

[e] *Gdansk University of Technology, Department of Electrochemistry, Corrosion and Materials Engineering, Narutowicza str. 11/12, 80-233 Gdansk, Poland*

[f] *Luleå University of Technology, Department of Engineering Sciences and Mathematics, Regnbågsallén, 97187 Luleå, Sweden*

Abstract

In this study, nanocrystalline Ni and Ni-diamond coatings were obtained by electrodeposition from tartrate electrolyte at ambient temperature to achieve good corrosion and wear resistance. Microhardness and adhesion tests respectively were performed for the wear resistance determination. Electrochemical impedance spectroscopy and linear polarization methods were used for corrosion resistance measurements and atomic force microscopy, and scanning electron microscopy were used for surface property characterization. The introduction of nanodiamond particles into the coating led to a rougher surface structure and a larger grain size in comparison with bare nickel coating. The study shows that the addition of $5 \cdot 10^{-2}$ ($g \cdot dm^{-3}$) of nanodiamonds to the plating bath is enough to obtain composite coatings with a clear increase in microhardness and wear resistance. The slightly improved corrosion resistance of the coating and decrease in corrosion current density from 0.41 to 0.14 $\mu A \cdot cm^{-2}$ in neutral chloride-containing medium, and nobler values of the corrosion potential were also observed.

Keywords: electrolytic co-deposition; Ni-nanodiamond composite coating; kinetics; morphology; corrosion; wear

1. Introduction

Electrodeposition of Ni-diamond composite coatings is a cheap and reliable way of surface modification to achieve desired properties, such as wear, corrosion resistance, abrasion resistance, and enhanced catalytic activity. Introduction of nanodiamond particles allows forming of fine-grained, dense, and low-porous coatings with improved hardness properties up to 2−5 times [1].

* Corresponding author
E-mail: Iryna.Makarava@lut.fi
DOI: 10.1016/j.surfcoat.2019.125063
Post-print of article published in journal Surface and coating technology (2019).

Moreover, such composite materials with increased hardness can potentially be used in production of cutting tools [2]. A good metallic matrix needs to possess satisfactory adhesion to the substrate, a high degree of growth of the second (inert) phase, and the possibility of thick coating deposition in order to produce such composite coating. Thus, Ni [3−7, 8], Co [9], Zn [10], Cu [11, 12] and their alloys (Co−W [13], Ni−Co [4, 14], Ni−Mo [15], Cu−Sn [16]) are among good candidates for such matrix materials.

There are several studies reporting successful co-deposition of nickel with a carbon-containing phase, in particular, graphite [17], carbon nanotubes [18], fullerenes [19, 20], and diamonds [1, 21–25]. Several studies report deposition of such diamond-containing composites under different conditions. In detail, nickel coatings containing diamonds of various sizes ranging from 4–6 nm [22, 23, 26], 10 nm [27, 28], 500 nm [24] to several microns were investigated. The content of diamond particles in the formed coatings ranged from tenths to several weight percent. Wang L. et al. [1] investigated co-deposition of nano-sized diamond particles from Watts electrolyte and showed no impact of nanodiamond particles on the crystal texture and structure of nanocrystalline Ni matrix. Also unexpected poorer wear resistance as compared with pure Ni coatings was observed. However, the amount of nanodiamonds was not varied and a large concentration of nanodiamond particles (10 $g \cdot L^{-1}$) in the plating bath was used. Such a large concentration can potentially hinder any improvement of nanomechanical properties. Thus, more studies are needed to investigate and elucidate the effect of nanodiamonds concentration and composite preparation on its mechanical, tribological, and corrosion properties. Often, quite high concentrations of the second phase particles are used in the composition of the plating bath as reported in other studies [24]. Such high concentration are used due to low amount of incorporated particles in Ni electrodeposits. The main issue for the co-deposition of Ni and nanodiamonds via electrodeposition is the low dispersion stability of the plating bath. This is due to high tendency for nanoparticles to agglomerate and sediment. Thus, obtaining of the Ni-diamond composite coatings is a challenging task but these negative effects can be minimized with using low concentration suspension of nanodimonds in the plating bath.

It was also shown that the ultradispersed diamond nanoparticles are of a shape close to oval or spherical without sharp edges and possess a combination of unique properties, such as a large specific surface area (up to 450 m^2), high surface energy, and a complex structure. This structure is presented in Fig. 1*a* as a sketch [29, 30] with the classical cubic diamond core (size of ~ 40 Å) and the carbon shell containing amorphous carbon structures (4–10 Å). This shell consists of sp^2-hybridized carbon atoms with oxygen-containing functional groups. The non-diamond

* Corresponding author
E-mail: Iryna.Makarava@lut.fi
DOI: 10.1016/j.surfcoat.2019.125063
Post-print of article published in journal Surface and coating technology (2019).

components of pure nanodiamond particles are a part of the produced material, and is affecting the bulk material properties [31].

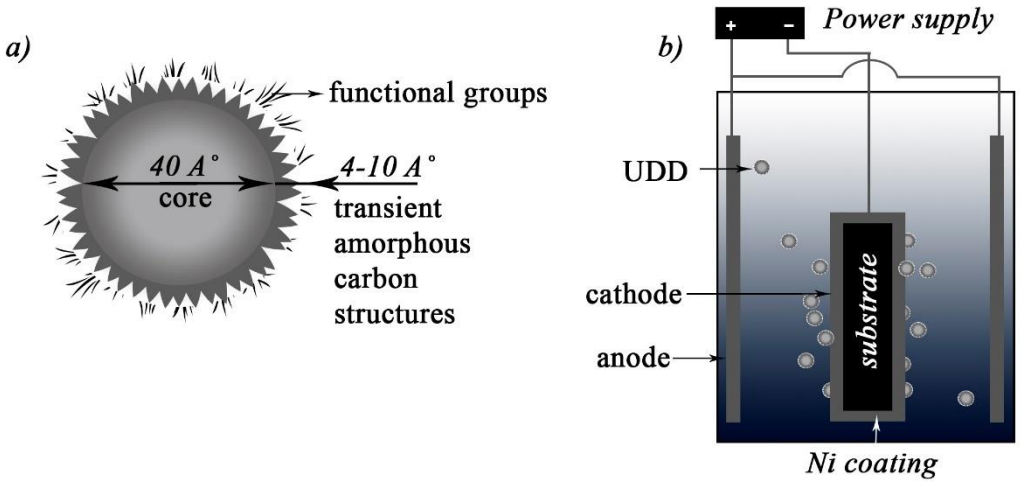

Fig. 1. Schematic illustration of nanodiamonds structure (*a*) and their co-deposition during cathodic electrodeposition of metals; Scheme of the electrodeposition (*b*)

The size of the crystallites (grain) in the matrix has a large influence on the physico-mechanical properties of the resulting coating [11]. Nickel belongs to a group of metals allowing the formation of fine crystalline adhesive coatings [32–34]. Commonly used electrolyte for the electrodeposition of nickel coatings is a mixture of nickel sulfate and nickel chloride with the addition of boric acid as a buffer additive (Watts electrolyte) [35, 36]. The solution is operated at elevated temperature (50–55 ºC), otherwise, it is impossible to achieve current efficiency close to 100% during deposition. The elevated temperature leads to fast evaporation of electrolyte, necessity of additional time for electrolyte heating, and control of temperature during electrolysis [25]. In our previous works [25, 37, 38], it was shown that replacing the buffer and complexing additive H_3BO_3 in nickel-plating electrolytes with organic components (acids and salts) allowed the formation of Ni coatings with desired functional and performance properties at ambient temperatures. This work is a continuation of our previous study [25] on the electrodeposition of Ni-based composite coatings from electrolytes at an ambient temperature with extension on mechanical, tribological, and corrosion properties of the nanodiamond particles-containing coatings. In particular, the effect of nanodiamond concentration on these properties and also on the composition and structure of the coatings has been studied.

2. Experimental

2.1. Sample preparation and coating electrodeposition

* Corresponding author
E-mail: Iryna.Makarava@lut.fi
DOI: 10.1016/j.surfcoat.2019.125063
Post-print of article published in journal Surface and coating technology (2019).

The electrodeposition of composite nickel–nanodiamonds coatings was performed from a tartaric bath at ambient temperature. During the electrodeposition, carbon steel or copper plates were used as the cathode and a pure Ni plate was used as the anode. The analytical reagent grade chemicals were dissolved in distilled water to form the plating bath solution. Cathodes were mechanically ground with #1200 and #2000 emery paper and then suspended in a degreasing bath containing, (in $g \cdot dm^{-3}$): Na_2CO_3 − 30, $Na_3PO_4 \cdot 12H_2O$ − 30, NaOH − 40 at 60−80 ºC. Copper plates were additionally electrochemically treated cathodically in a degreasing bath, (in $g \cdot dm^{-3}$): Na_2CO_3 − 30, $Na_3PO_4 \cdot 12H_2O$ − 30 at 50−60 ºC for 1−2 min at a current density of 1 ($kA \cdot m^{-2}$). After that, the sheets were chemically etched in 0.1 M sulfuric acid at ambient temperature in order to obtain the contamination-free surface.

The bath composition and its operating conditions are listed in Table 1. The schematic representation of the electrochemical electrodeposition of a composite coating is shown in Fig. 1, *b*. The Rochelle salt ($KNaC_4H_4O_6 \cdot 4H_2O$) concentration during electrodeposition was 0.2 ($mol \cdot dm^{-3}$). In order to study the kinetic features of nickel oxidation and reduction in the presence of nanodiamond particles, the concentration of $KNaC_4H_4O_6 \cdot 4H_2O$ was varied from 0.05 to 0.3 ($mol \cdot dm^{-3}$) and Ni^{2+} from 0.7 to 1.0 ($mol \cdot dm^{-3}$), respectively. The suspension bath was stirred by a mechanical stirrer at a stable rotational speed (300 rpm). Ultradispersed diamonds with an average nominal diameter of 6 nm obtained by denotational synthesis were received from«SINTA»(Belarus) as 5% dispersion and were used as the second phase without any further pretreatment. The temperature of the plating bath during the electrolysis was controlled by a 5 OK-20/0,05-02 water thermostat (5 Okeanov, Belarus) in a beaker with a jacket. After the plating process, the deposits were washed with distilled water and dried with a flow of air.

Table 1. Bath composition and electrodeposition parameters

Component/parameter	Value
$NiSO_4 \cdot 7H_2O$	0.8 ($mol \cdot dm^{-3}$)
$NiCl_2 \cdot 6H_2O$	0.2 ($mol \cdot dm^{-3}$)
Rochelle Salt	0.2 ($mol \cdot dm^{-3}$)
Nanodiamond Particles	up $5 \cdot 10^{-2}$ ($g \cdot dm^{-3}$)
Stirring Rate	300 (rpm)
Current Density	2 ($A \cdot dm^{-2}$)
Temperature	20−25 ºC

* Corresponding author
E-mail: Iryna.Makarava@lut.fi
DOI: 10.1016/j.surfcoat.2019.125063
Post-print of article published in journal Surface and coating technology (2019).

2.2. Surface analysis

A scanning electron microscope (JEOL JSM–5610 LV) and a Flex-Axiom atomic force microscope system (Nanosurf, Switzerland) were used to investigate the surface and cross-section morphology and topography. The AFM measurements were conducted in the tapping mode using an *n*-type silicon cantilever with a nominal tip radius of 8 nm (HQ:NSC15/Al, MikroMasch). The chemical composition of the coatings was identified by an energy-dispersive X-ray spectroscopy (EDS) system of the scanning electron microscope. The contact potential difference voltage (V_{CPD}) and phase mapping of reference nickel coating and coating containing $5 \cdot 10^{-2}$ ($g \cdot dm^{-3}$) of nanodiamond particles (concentration in electrolyte) were performed with Intermodulation AFM (ImAFM) and Intermodulation Electrostatic Force Microscopy (ImEFM) on a Bruker Dimension Icon AFM (Bruker, USA) connected to a multi-frequency lock-in amplifier (Intermodulation Products AB, Sweden). More details on the ImAFM and ImEFM techniques can be found in [39, 40]. The data were analyzed using the IMP software suite (version 1.1, Intermodulation Products AB) and processed with Gwyddion software [41] (version 2.44). The measurements were conducted using NCH-20 (with platinum coating) probes with a nominal spring constant of 42 N/m. The ImEFM measurements were taken at 1 Hz acquisition speed and the measured areas contain 256×256 data points.

A D8 Advance AXS X-ray diffractometer (Bruker, Germany) with Cu *K*α radiation (λ= 0.15418 nm) was employed to obtain XRD spectra. The XRD spectra were analyzed by Match! software. The average grain diameter was calculated using the Scherrer equation, as follows:

$$d = \frac{0,9 \cdot \lambda}{b \cdot \cos\theta}, \quad (1)$$

where b is the FWHM, θ is the diffraction angle, d is the grain size, and λ (0.15405 nm) is the wavelength of the radiation used.

2.2. Mechanical and tribological studies

The microhardness of the obtained coatings was tested by a Vickers hardness indenter (Matsuzawa MXT-CX) with a load of 100 g for 15 s. Each microhardness value was calculated as an average of ten measurements.

The wear resistance of the coatings was examined under the dry sliding condition in air at 25 C for 30 min by the pin-on-disk method. All wear tests were performed against 7 mm diameter ruby balls under the load of 1 N at a fixed rotation speed of 200 rpm. For each type of sample, three tests were carried out under the same conditions. After the wear test, worn surface morphology was evaluated using optical microscopy.

* Corresponding author
E-mail: Iryna.Makarava@lut.fi
DOI: 10.1016/j.surfcoat.2019.125063
Post-print of article published in journal Surface and coating technology (2019).

Adhesion of the coatings was obtained with an adhesivemeter (PosiTest AT-A). Substrates with Ni and Ni-nanodiamond coatings were glued to the surface of aluminum support with a diameter of 20 mm. Then the tensile test was performed.

2.3. Electrochemical measurements

Electrochemical measurements were carried out in a three-electrode cell with saturated silver/silver-chloride electrode as a reference electrode, platinum wire as a counter electrode, and nickel or a copper substrate with electrodeposited nickel–nanodiamond coating (exposed surface area 1 cm^2) as a working electrode using an Autolab PGSTAT 302N potentiostat-galvanostat (Methrom Autolab, The Netherlands). In order to study the influence of nanodiamonds on the deposition kinetics and oxidation, diamond particles were added to electrochemical set-up. Prior to experiments, working electrodes were immersed in the electrolyte for 30 min with the moment of immersion set as zero. Potentiodynamic polarization was carried out at a 5 ($mV \cdot s^{-1}$) sweep rate in both cathodic and anodic directions. The temperature was controlled by a water jacket using a liquid thermostat. The solution pH was adjusted to 2 using 0.1 M H_2SO_4.

From the linear polarization curves of nickel electrode, common kinetic parameters of oxidation and reduction process were determined. The open circuit potentials (OCP) were recorded 60 minutes after adjustment of the current at increasing and decreasing current densities until reproducible values were achieved. By linear fitting of Tafel η–log *i* curves (Eq. 2), the Tafel slope (*b*) (Eq. 3), of the curves was obtained.

$$\eta = -\frac{2{,}303RT}{\alpha nF} log i_0 - \frac{2{,}303RT}{\alpha nF} log i = a + b log i, \quad (2)$$

$$b = -\frac{2{,}303RT}{\alpha nF}, \quad (3)$$

where η is the overpotential (V), b is the Tafel slope (V $decade^{-1}$), α is the transfer coefficient, and i is the current density (A cm^{-2}). The exchange current densities i_o for nickel deposition were found by extrapolating the Tafel regions to zero overpotential

According to Tafel formula (eq. 2) the equation $log i_0 = \frac{a}{b}$ can be deducted. The charge transfer coefficient (α) was calculated using the following equation $\alpha = -\frac{2{,}303RT}{bnF}$.

To determine the susceptibility of obtained Ni and Ni-nanodiamond coatings to localized corrosion in aqueous 0.5 M NaCl solution (chloride environment) linear polarization measurements were performed at room temperature with 1 ($mV \cdot s^{-1}$) sweep rate according to ASTM G 61-86. Electrochemical impedance spectroscopy (EIS) spectra were recorded at OCP in

* Corresponding author
E-mail: Iryna.Makarava@lut.fi
DOI: 10.1016/j.surfcoat.2019.125063
Post-print of article published in journal Surface and coating technology (2019).

an applied frequency ranged from 10 kHz down to 0.01 Hz with a wave amplitude of 10 (mV). All measurements were at least triplicated.

3. Results and discussion

3.1 Kinetics of nickel electrodeposition and dissolution in the presence of nanodiamond particles

Figure 2 shows the effect of the second phase (nanodiamonds) introduction on the cathodic (Fig. 2, *a*) and anodic (Fig. 2, *a*, *b*) polarization of nickel electrode in tartrate electrolyte. This allows kinetic characterization of nickel reduction and oxidation, respectively.

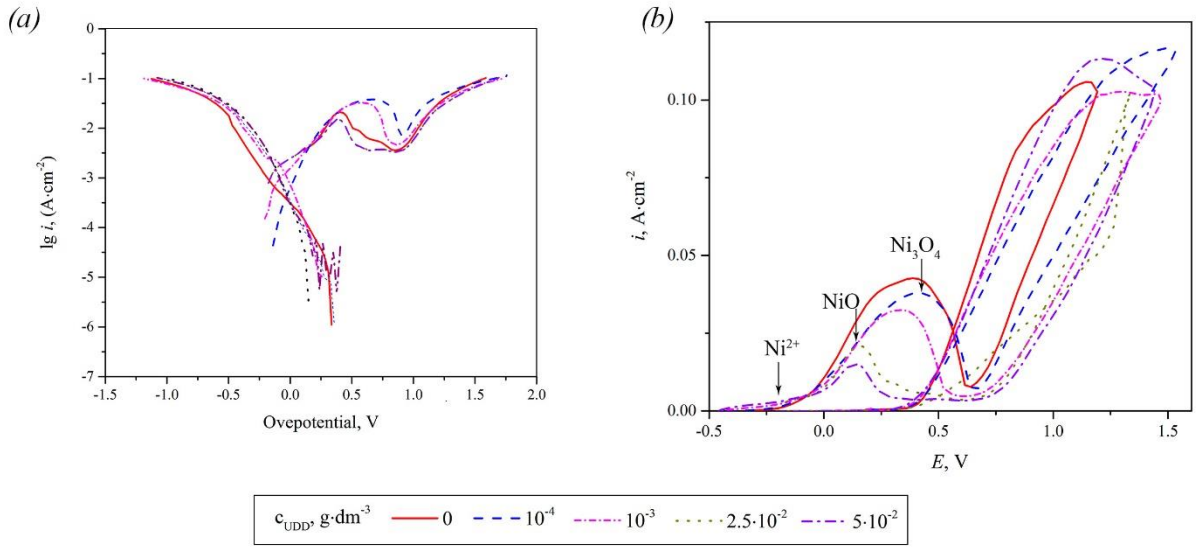

Fig. 2. Cathodic and anodic curves in Tafel coordinates (*a*) and anodic (*b*) polarization curves of nickel electrode in the presence of nanodiamond particles (potentials vs SHE).

The OCP (Fig. 2, *a*) remained almost unchanged with nanodiamonds addition in the electrolyte. On the other hand, the presence of nanodiamond particles leads to an increase in cathodic polarization. This is probably due to the adsorption of nanodiamonds on the surface of the cathode that impedes the reduction of nickel ions with a decrease in active surface area of cathode [18]. Such trends were also observed for similar systems [10].

The main kinetic parameters of the nickel electrode were calculated from the linear polarization curves (Fig. 2) and are presented in Table 2. The abscissa of each polarization curve in Fig. 2 is subtracted from the respective OCP, then multiplied by −1, and transformed to the

* Corresponding author
E-mail: Iryna.Makarava@lut.fi
DOI: 10.1016/j.surfcoat.2019.125063
Post-print of article published in journal Surface and coating technology (2019).

overpotential. On the basis of the above, the ordinate of each curve is divided by the electrode area and multiplied on current efficiency, and their logarithms were formed. The resulting partial cathodic Tafel curves of Ni electrodeposition at different concentrations of nanodiamond particles are presented as the inset in Fig. 2, *a*.

Table 2 Kinetic parameters of nickel reduction and oxidation in tartaric electrolyte with nanodiamond particles addition

C, $g \cdot dm^{-3}$	Cathodic branch (±0,005 V)		Anodic branch (±0,005 V)		α_c	i_o, $A \cdot m^{-2}$
	a, V	$\lvert b \rvert \cdot$dec, V	a, V	$b \cdot$dec, V		
0	−0.495	0.145	1.445	0.506	0.03	$1.78 \cdot 10^{-2}$
$1 \cdot 10^{-4}$	−0.220	0.137	0.655	0.259	0.22	$2.83 \cdot 10^{-2}$
$1 \cdot 10^{-3}$	−0.187	0.131	0.626	0.277	0.23	$3.18 \cdot 10^{-2}$
$2{,}5 \cdot 10^{-2}$	−0.257	0.136	0.330	0.159	0.05	$2.11 \cdot 10^{-2}$
$5 \cdot 10^{-2}$	−0.178	0.132	0.405	0.231	0.22	$4.20 \cdot 10^{-2}$

Coefficient *b* during the reduction of nickel was between –0.13 and –0.14 V both in the electrolyte with and without the nanodiamond addition, testifying the invariance of the electroplating process and corresponding that the attachment of the first electron is the limiting stage of the process [42]. Thus, the limiting stage of nickel ion reduction in the potential range from –0.4 to –0.8 V is the electron transfer stage and, therefore, the addition of nanodiamond particles does not change Ni^{2+} reduction mechanism, which can be shown with the following steps:

$$Ni^{2+} + e^- \rightarrow Ni^+ \text{ (limiting stage)} \quad (4)$$

$$Ni^+ + e^- \rightarrow Ni \quad (5)$$

The current density of electrodeposition of nickel increases from $1.78 \cdot 10^{-2}$ to $4.20 \cdot 10^{-2}$ ($A \cdot m^{-2}$) with an increase of nanodiamond concentration in the electrolyte from 0 to $5 \cdot 10^{-2}$ ($g \cdot dm^{-3}$). The exchange current density i_0 usually increases when the electrochemical reaction is accelerated [43]. This increase of reaction rate implies that nanodiamond particles accelerate the rate of Ni^{2+} ion transfer across the electrical double layer. The accelerating effect of nanodiamond particles could be due to their adsorption capability [44] on cathode and changing of the surface area.

The beginning of the nickel oxidation process (Fig. 2, *b*, Eq. 6) is observed at more noble potentials than (–0.25) V, besides, there is one oxidation peak in the potential range of 0.2–0.6 V. Also, there is a tendency of the oxidation peak to shift to the region of more electronegative values

* Corresponding author
E-mail: Iryna.Makarava@lut.fi
DOI: 10.1016/j.surfcoat.2019.125063
Post-print of article published in journal Surface and coating technology (2019).

with an increase of nanodiamonds concentration from 0 to $5 \cdot 10^{-2}$ ($g \cdot dm^{-3}$). This shift indicates the possibility of the processes described by Eq. (7) and Eq. (8) and also can indicate a possible change in the form of nickel oxide. It can be expected that Ni_3O_4 is forming due to the blocking of the electrode surface during adsorption of nanodiamond particles and the local decrease in i_{peak} [42].

$$Ni \rightarrow Ni^{2+} + 2e^- \qquad E° = -0.250\ V \quad (6)$$

$$Ni + H_2O = NiO + 2H^+ + 2e^- \qquad E° = 0.11\ V \quad (7)$$

$$3Ni + 4H_2O = Ni_3O_4 + 8H^+ + 8e^- \qquad E° = 0.307\ V \quad (8)$$

3.2 Structure characteristics and properties of nickel and nickel-nanodiamond coatings

Diffractograms of nickel and nickel-nanodiamond coatings for 2θ ranging 40–80° are presented in Fig. 3.

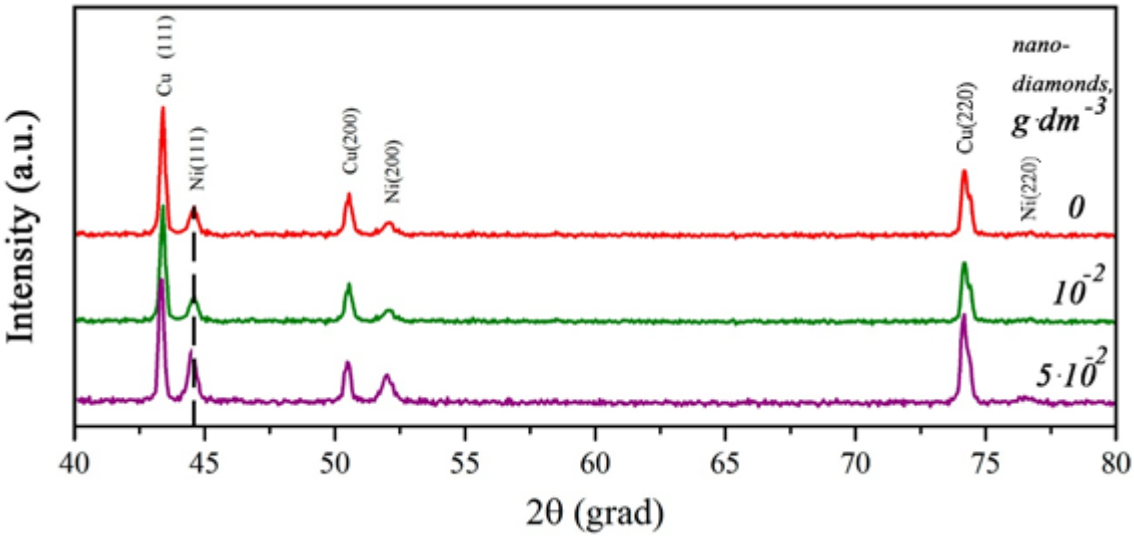

Fig. 3. XRD patterns of nickel and nickel-nanodiamond coatings (concentration of nanodiamonds in the electrolyte is indicated).

The peaks corresponding to copper and nickel were detected in the presented diffractograms. These peaks represent the data measured for the Cu substrate and the Ni coating. There is a tendency for the diffraction peaks broadening approximately about 20% for both Ni and Cu at (111) and (200) with an increase in the nanodiamond content to $5 \cdot 10^{-2}$ ($g \cdot dm^{-3}$). A peak of higher intensity for the nickel at about 44.5 degrees corresponds to (111) plane, at 52.2 degrees

* Corresponding author
E-mail: Iryna.Makarava@lut.fi
DOI: 10.1016/j.surfcoat.2019.125063
Post-print of article published in journal Surface and coating technology (2019).

corresponds to the (200) plane, and peak of small intensity at 77.2 degrees corresponds to the (220) plane. These peaks are sensitive to the addition of nanodiamonds and their broadening also validates the change in nanodiamond particles concentration in the coatings. Thus, it can be concluded that nanodiamond particles modify the structure of Ni matrix [15]. Similar results were also found for other systems [3, 18]. The absence of nanodiamond diffraction peaks is due to the low (<5%) concentration which is below the detection limit. Note, that the EDS analysis revealed peak at 0.3 keV, which can be associated with carbon-based (nanodiamond particles) species in the coating (as shown in the supplementary Fig. S1).

The nanodiamond addition influences the size of the nickel crystal in the formed coatings. Increasing of nanodiamond concentration in the electrolyte from 0 to $5 \cdot 10^{-2}$ ($g \cdot dm^{-3}$) is accompanied by a slight increase in the size of Ni crystals from 16.3 to 22.5 nm, as estimated using the Scherrer equation (1). The Ni crystalline size depends on the nanodiamond concentration and can be associated with the different rates of metal nucleus growth during the coating electrodeposition. The nanodiamond particles are uniformly distributed in the solution and are adsorbed in the growing nickel matrix with a slight increase in the crystal growth and thus decreasing the nucleation [45]. Besides, addition of nanodiamond particles can increase defects in crystal structure and thus affect its size [46, 47]. With other hand, addition of nanodiamond particles influencing crystallization and can increase current exchange. Thus, quantity of formed crystals would be reduced with a possible increase in their sizes.

3.3 Surface characteristics of nickel and nickel- nanodiamond coatings

The morphology of the coating surfaces has changed with addition of nanodiamond particles as shown in the SEM images (Fig. 4). Electrodeposition of nickel and composite coating with nanodiamonds at the concentration of 0.001 ($g \cdot dm^{-3}$) in the electrolyte allowed the formation of a uniform fine-crystalline coating with crystal sizes of about 0.1–0.2 μm. The increase of nanodiamonds concentration to $5 \cdot 10^{-2}$ ($g \cdot dm^{-3}$) led to the coarsening of particles and formation of structures with sizes of about 0.4–0.7 μm.

* Corresponding author
E-mail: Iryna.Makarava@lut.fi
DOI: 10.1016/j.surfcoat.2019.125063
Post-print of article published in journal Surface and coating technology (2019).

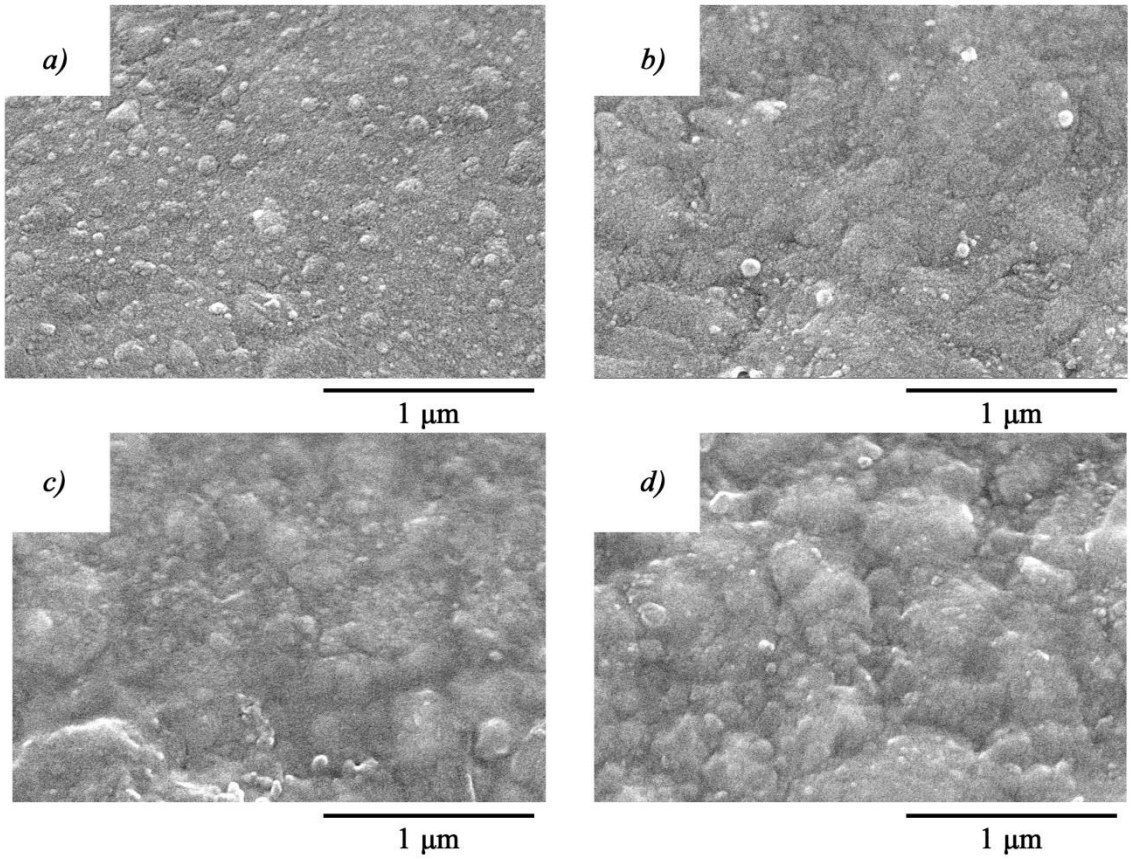

Concentration of nanodiamonds in electrolyte, ($g \cdot dm^{-3}$): *a* – 0, *b* – $1 \cdot 10^{-3}$; *c* – $1 \cdot 10^{-2}$; *d* – $5 \cdot 10^{-2}$

Fig. 4. SEM images of Ni (*a*) and Ni- nanodiamond (*b*-*d*) coatings

The presence of $5 \cdot 10^{-2}$ ($g \cdot dm^{-3}$) nanodiamonds (Fig. 4, *d*) in the electrolyte caused significant agglomeration of nanodiamonds (up to 2–5 μm) and it was also observed in our previous work [25].

The cross-sections of pure Ni and Ni- nanodiamond coatings are shown in Fig. 5.

* Corresponding author
E-mail: Iryna.Makarava@lut.fi
DOI: 10.1016/j.surfcoat.2019.125063
Post-print of article published in journal Surface and coating technology (2019).

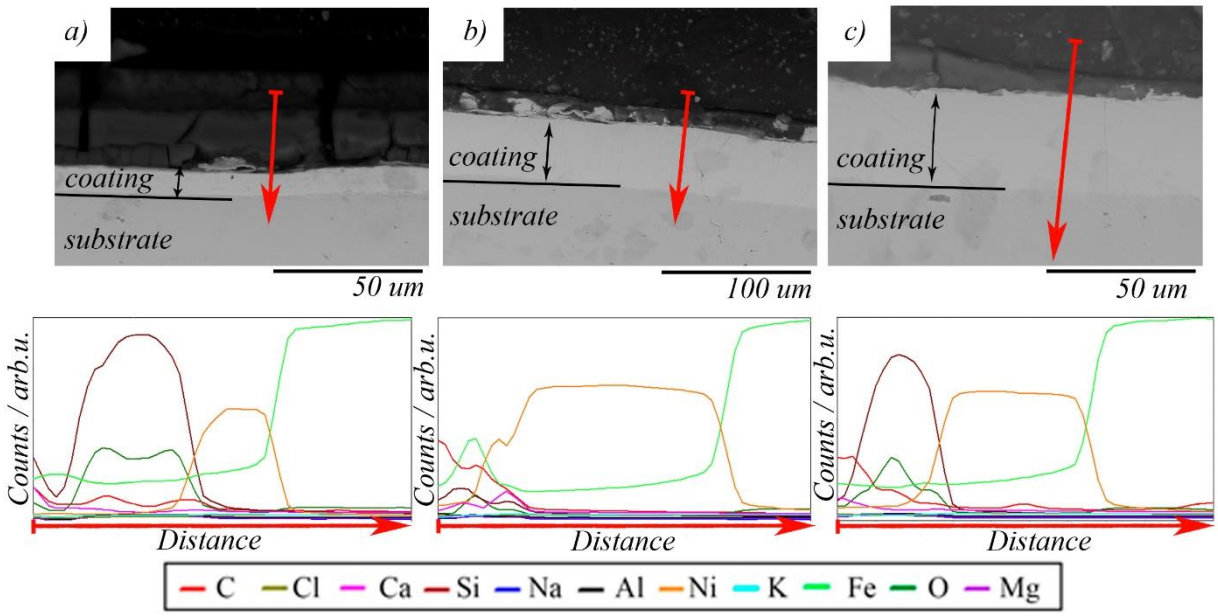

Concentration of nanodiamonds in electrolyte, ($g \cdot dm^{-3}$): *a* – 0; *b* – $1 \cdot 10^{-2}$; *c* – $5 \cdot 10^{-2}$

Fig. 5. Microphotographs of cross-sections and corresponding elemental distribution (red arrow shows place and direction of the scan). The place where Ca, Si, Al and Mg were identified is substrate of cross-section (resin).

Ni and Ni-nanodiamond coatings have a homogeneous distribution with clear lines between the substrate and coating which suggest a good adhesion. The good adhesion between the coating and substrate is demonstrated later in the adhesion measurements section (Table 3).

The roughness of the initial Ni coating and Ni coating containing $5 \cdot 10^{-2}$ ($g \cdot dm^{-3}$) nanodiamond particles was evaluated with AFM. The measured topography maps with the corresponding roughness cross-sections are shown in Fig. 6. There is some tendency for the roughness increase of the nanodiamond-containing coatings in comparison with the pure coating due to possible nanodiamonds agglomeration in the electrolyte as previously reported in [12].

* Corresponding author
E-mail: Iryna.Makarava@lut.fi
DOI: 10.1016/j.surfcoat.2019.125063
Post-print of article published in journal Surface and coating technology (2019).

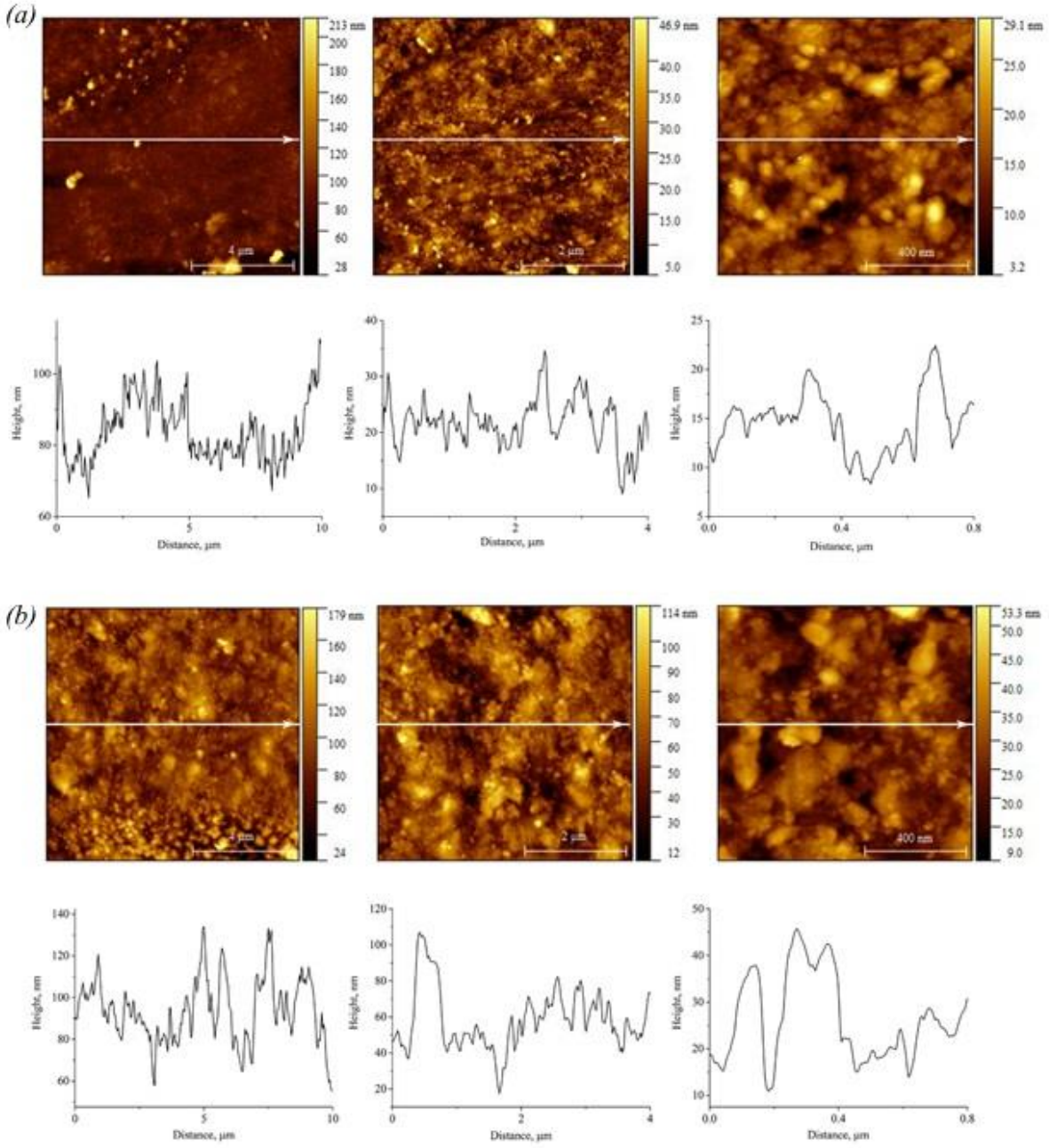

Concentration of nanodiamonds in electrolyte, ($g \cdot dm^{-3}$): *a* – 0; *b* – $5 \cdot 10^{-2}$

Fig. 6. AFM topography images of nickel (*a*) and nickel-nanodiamond (*b*) coatings and corresponding roughness profiles along the lines indicated in the AFM images.

The average roughness (R_a) was evaluated for all three studied areas and is presented in Table 3. Higher concentration of nanodiamond particles in the electrolyte leads to a higher roughness and microhardness of the coatings obtained as reported in Table 3.

* Corresponding author
E-mail: Iryna.Makarava@lut.fi
DOI: 10.1016/j.surfcoat.2019.125063
Post-print of article published in journal Surface and coating technology (2019).

Table 3. Properties of nickel and nickel-nanodiamond coatings (concentration of nanodiamonds in electrolyte $5 \cdot 10^{-2}$ ($g \cdot dm^{-3}$)).

		Nickel	Nickel- nanodiamond
Roughness R_a, nm	10×10 μm	3.04	7.27
	4×4 μm	2.71	7.55
	0.8×0.8 μm	1.14	3.23
Coating Microhardness, HV	surface	198	306
	cross-section	280	450
Adhesion (the maximum applied load), MPa		1.2 MPa	1.2 MPa

The presence of $5 \cdot 10^{-2}$ ($g \cdot dm^{-3}$) nanodiamonds in the nickel-plating electrolyte contributes to a 1.5-times increase in the microhardness compared to the bare nickel coating. The microhardness of the cross-section reaches 450 HV and slightly changes along the length of the thin section. This might indirectly indicate about possible uniform distribution of the second phase in the matrix. This observation can be explained by surface texture changes of nickel and composite hardening due to addition of the nanodiamond particles [4]. The adhesion of nickel and composite coatings to the substrate is similar and satisfactory. The coatings can withstand the maximum applied load adhesion 1.2 MPa (tension test by PosiTest AT-A method) at what no coating damage was observed. After this load support is detached from the substrate.

The obtained coatings were examined for the surface robustness via the wear tests. The results of wear tests in dry conditions are shown in Fig. 7.

* Corresponding author
E-mail: Iryna.Makarava@lut.fi
DOI: 10.1016/j.surfcoat.2019.125063
Post-print of article published in journal Surface and coating technology (2019).

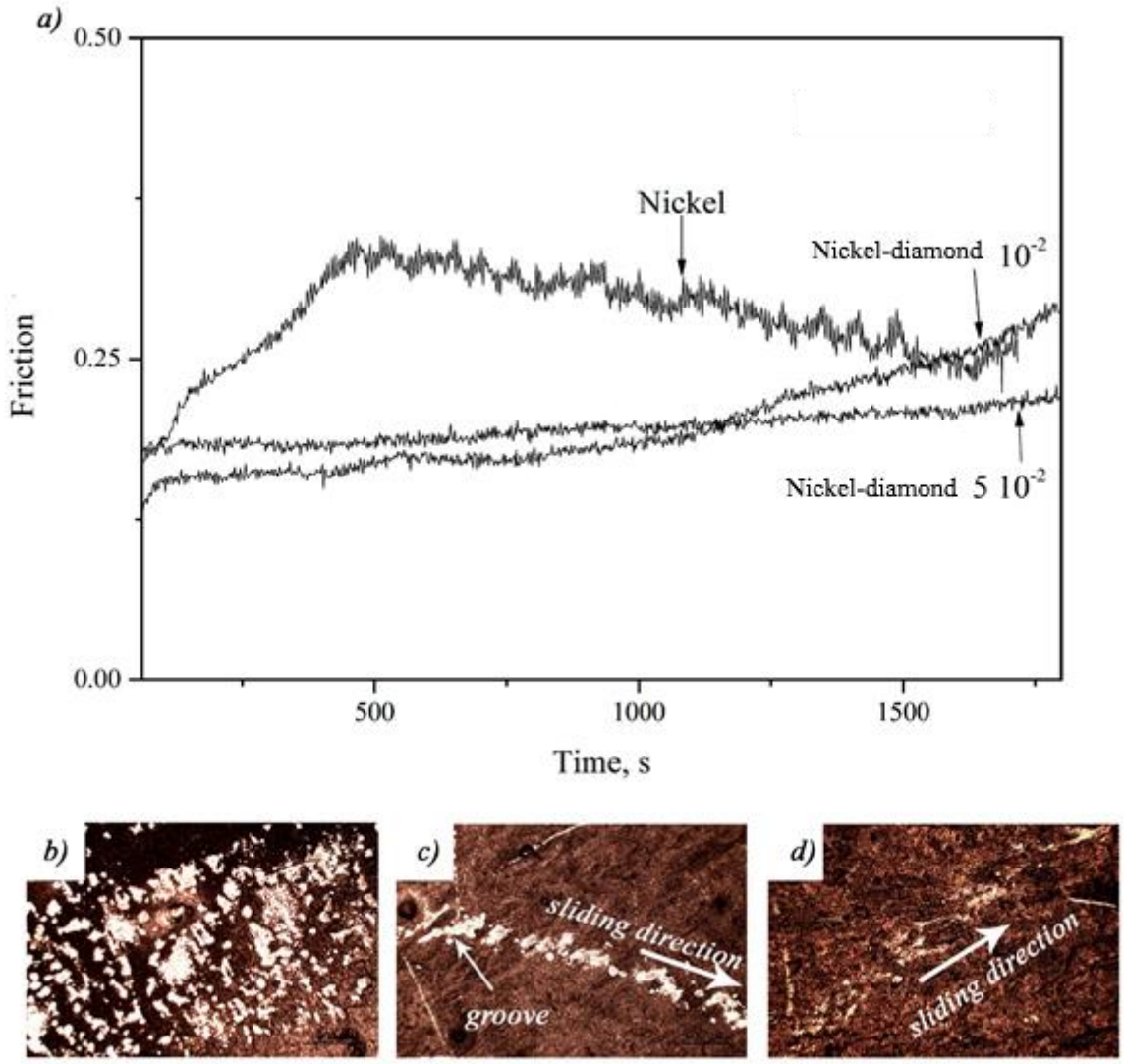

Nanodiamonds concentration in electrolyte, (g·dm^{-3}): *a* – 0; *b* – 10^{-2}; *c* – $5 \cdot 10^{-2}$

Fig. 7. Coefficient of friction versus sliding distance curves, obtained for nickel and nickel-nanodiamond composite coatings (*a*) and optical micrographs of wear scars (*b–d*)

The influence of the nanodiamond content on the wear of the coatings was studied and it was revealed that the wear resistance of the composite coatings was enhanced. A lower wear rate is observed for the nanodiamond-containing coatings as compared with the bare nickel coating. This is connected to the addition of nanodiamond particles and the increased hardness of the nickel-plating coating, which leads to an improved wear resistance of the composite coatings. As the result, the friction coefficient of composite coating was reduced. At the initial stage of testing (run-in stage), the friction coefficient of pure nickel coating is about 0.18. The friction coefficient has gradually increased to 0.33–0.34 after 400 s with a slight decrease to 0.28–0.30 after 500 s.

* Corresponding author
E-mail: Iryna.Makarava@lut.fi
DOI: 10.1016/j.surfcoat.2019.125063
Post-print of article published in journal Surface and coating technology (2019).

The friction coefficient for the nanodiamond-contained nickel coatings remained almost constant up to about 1000 s following with a slight increase up to 0.20. This increase of the friction at the later stage (ca. 1500 s) is possibly due to occurrence of the abrasive wear. The measured friction was lower for the nanodiamond-containing coatings than for the pure Ni coating. Thus, former have better tribological properties and addition of nanodiamonds can have a lubricating effect. Optical micrographs of wear scars reveal clear smooth traces of wear machine. The groove of sliding is less visible for the nanodiamond-containing coatings (Fig. 7 *d*).

The ImEFM technique was applied to identify nanodiamond particles or possible clusters in the nickel matrix, as shown in Fig. 8. To distinguish such small nanoparticles of 10 nm sizes in the matrix is a challenging task. Topographical images measured with AFM are often not sensitive to different material properties and thus such small nanoparticles will show no difference in contrast. On the other hand, phase imaging in tapping mode and more advanced AFM methods such as PeakForce quantitative nanomechanical mapping (PeakForce QNM) can potentially be applied. However, the elastic modulus of nickel is very high and would require the use of an AFM cantilever with a very high spring constant and expensive diamond tip. Thus, a better option is to map these nanoparticles by differences in their surface potential, or measured V_{cpd}, with ImEFM offering high potential and lateral resolution. For the reference nickel coating containing no nanodiamonds, the phase (Fig 8, 1 *a* and 1 *b*) and surface potential images (Fig 8, 2 *a* and 2 *b*) measured by ImEFM do not show any clear nanoparticles. The areas with lower negative potential, as expected for nickel, are possibly related to different surface oxide thickness. Also, these particle-like areas are of sizes larger than 100 nm. The corresponding topographical images (Fig 8, 3 *a* and 3 *b*) for the reference nickel coating demonstrate no clear topography since the measurement setpoint, i.e. scanning normal force, was optimized to minimize a possible cross-talk between surface topography and the measured potential. The scanning normal force in ImEFM measurements was increased to image the nanodiamond particles in the nanocomposite containing $5{\cdot}10^{-2}$ ($g{\cdot}dm^{-3}$) nanodiamond particles. This was probably due to the presence of an oxide film on the surface hindering nanoparticle identification. Clear small areas with a positive surface potential can be observed in the V_{cpd} images measured on the nanocomposite surface, as shown in Fig. 8 (2 *c* and 2 *d*). Figure 2, *d* is a repeat scan of the same location and highlights the same small areas. These areas are of sizes ranging in between 10−20 nm and can potentially be identified as nanodiamond particles. Also, the phase images measured simultaneously in ImAFM and sensitive to surface stiffness demonstrate different phase change for these small nanoparticles, as shown in Figure 8 (1 *c* and 1 *d*). This is an interesting result that ImAFM method can distinguish two such hard materials at nanoscale. The topography images for the nanocomposite are shown in Figure 8

* Corresponding author
E-mail: Iryna.Makarava@lut.fi
DOI: 10.1016/j.surfcoat.2019.125063
Post-print of article published in journal Surface and coating technology (2019).

(3 *c* and 3 *d*). The surface features are well seen due to higher imaging force, which also leads to the unwanted cross-talk between topography and potential. Thus, these measurements should be considered more qualitative than quantitative with the main aim to visualize such small nanoparticles in this nanocomposite. This can be of importance for further studies.

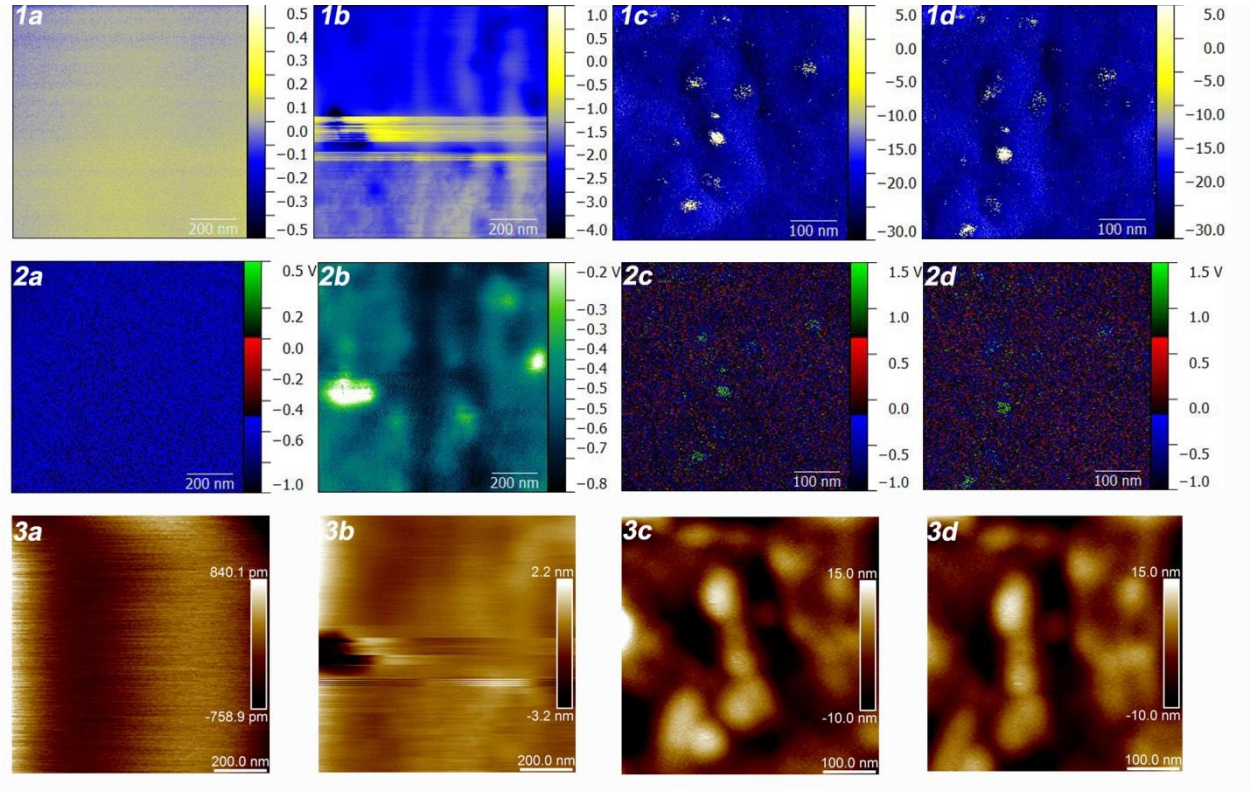

Fig. 8. The phase images measured by ImAFM for the reference nickel coating are in (1 *a*, *b*) and for the nanocomposite with $5 \cdot 10^{-2}$ ($g \cdot dm^{-3}$) nanodiamond concentration in electrolyte are in (1 *c*, *d*). The measured maps of potential distribution for the reference surface are shown in (2 *a*, *b*) and for the nanocomposite are in (2 *c*, *d*). The corresponding topographical images measured for the nickel coating are in (3 *a*, *b*) and for the nanocomposite are in (3 *c*, *d*).

3.2 Corrosion resistance of nickel and nickel-nanodiamond *coatings*

Potentiodynamic polarization curves of Ni and Ni-nanodiamond coatings obtained in 0.5 M NaCl solution are shown in Fig. 9. The electrochemical corrosion parameters, calculated from the analysis of the polarization curves, are given in Table 4. As can be seen from the presented data, nanodiamonds had a notable effect on corrosion properties of the coatings under study. Polarization curves of Ni-nanodiamond coatings obtained from the electrolyte containing 10^{-3} ($g \cdot dm^{-3}$) nanodiamonds were similar to those of pure Ni coatings, however, a repeatable difference of the cathodic branch of the polarization curve was observed. This can be due to the introduction

* Corresponding author
E-mail: Iryna.Makarava@lut.fi
DOI: 10.1016/j.surfcoat.2019.125063
Post-print of article published in journal Surface and coating technology (2019).

of the nanodiamonds second phase, which is cathodic in its nature relative to Ni. Nevertheless, corrosion potential and current density of these samples were quite similar. Further increase in the nanodiamond concentration to 10^{-2} (g·dm^{-3}) resulted in a noticeable shift (ca. −0.135 mV) of the corrosion potential to the anodic region, indicating higher corrosion resistance of the surface and corrosion current density, in this case, decreased ca. 5.5 times as compared to nanodiamond-free coating. Coatings obtained in the electrolyte containing 5 10^{-3} (g·dm^{-3}) nanodiamonds showed higher corrosion potential but also higher corrosion current density, most probably due to the changes in the microstructure of the electrode surface.

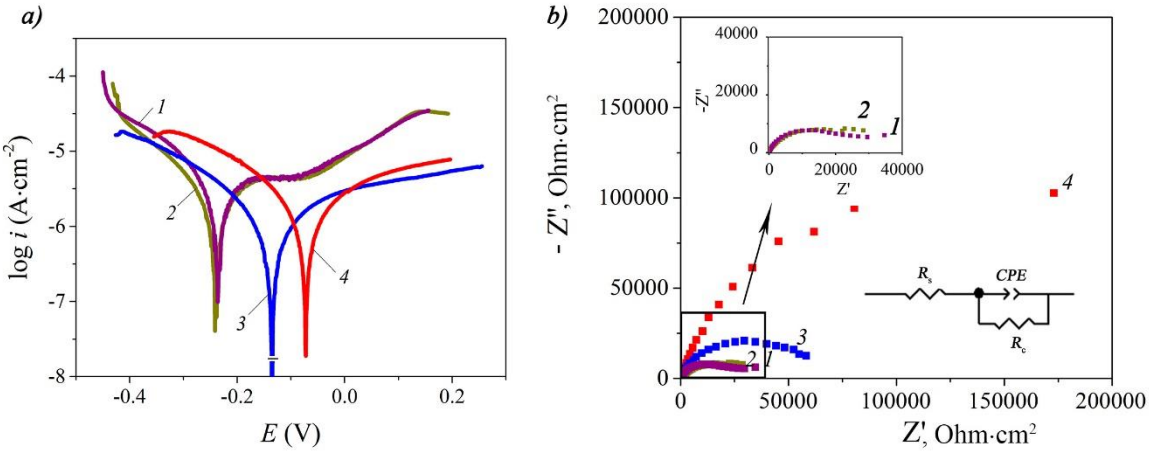

Concentration of nanodiamonds in electrolyte, (g·dm^{-3}): 1 – 0; 2 – 10^{-3}; 3 – 10^{-2}; 4 – $5{\cdot}10^{-2}$

Fig. 9. Potentiodynamic polarization curves of Ni and Ni-nanodiamond coatings in 0.5 M NaCl (*a*) Nyquist EIS plots in 0.5 M NaCl solution. Equivalent circuit, used for data analyzes is shown in (*b*) and the zoomed-in area is shown as an inset.

Table 4. Electrochemical parameters extracted from the potentiodynamic polarization curves

Concentration of nanodiamonds in electrolyte, (g·dm^{-3})	a_a, V	b_a·dec, V	a_c, V	$\|b_c\|$·dec, V	i_{corr}, μA·cm^{-2}	E_{corr}, V
0	0.0388	0.0073	−0.0326	0.4491	0.41	−0.241
10^{-3}	0.0290	0.0505	−0.0235	0.3875	0.38	−0.235
10^{-2}	0.0263	0.0489	−0.0148	0.2442	0.07	−0.135
$5{\cdot}10^{-2}$	0.0227	0.0848	−0.0245	0.2393	0.14	−0.073

* Corresponding author
E-mail: Iryna.Makarava@lut.fi
DOI: 10.1016/j.surfcoat.2019.125063
Post-print of article published in journal Surface and coating technology (2019).

Nyquist plots of bare nickel and nickel-nanodiamond composite coatings are presented in Fig. 8 and fitting parameters of the impedance experiments are listed in Table 5. The obtained spectra presented one capacitive time constant in the form of semi-circle. The impedance spectra were analyzed using equivalent circuit including R_c as charge transfer resistance, CPE element imitates the capacitive behavior of the electrical double layer, and R_s as the solution resistance.

Table 5. Parameters obtained from the fitting of the experiment impedance spectra after exposure to 0.5 M NaCl

	Concentration of nanodiamonds in electrolyte, ($g \cdot dm^{-3}$)			
	0	10^{-3}	10^{-2}	$5 \cdot 10^{-2}$
R_s, $\Omega \cdot cm^2$	20.89	18.43	17.82	23.55
Y_1, $s^n/(\Omega \cdot cm^2)$	$4.82 \cdot 10^{-5}$	$6.61 \cdot 10^{-5}$	$3.06 \cdot 10^{-5}$	$3.20 \cdot 10^{-5}$
n	0.87	0.71	0.82	0.84
R_c, $k\Omega \cdot cm^2$	22.36	27.76	58.57	283.99

The EIS results obtained in 0.5 M NaCl show an increase in the charge transfer resistance that indicates improved corrosion resistance of the composite coatings compared with the bare nickel coating. The highest R_c value (283.99 ($k\Omega cm^2$)) was obtained for the coating deposited from the bath containing $5 \cdot 10^{-2}$ ($g \cdot dm^{-3}$) of nanodiamonds. Quasicapacitive parameter (Y_1) does not change much with the impedance increase. This indicates an alteration of the relaxation time. The parameter n ($-1 \leq n \leq 1$) can be used to determine the degree of heterogeneity of the surface. The inclusion of nanodiamonds in nickel coatings leads to decreasing of this parameter that indirectly means changing in crystallization process, but it gives some variance as the smallest concentration allows to obtain the smallest parameter *n*. But it was shown that all properties changing in order during increasing of nanodiamonds concentration. Other authors state variation of impedance parameters n for coatings with different concentrations during the corrosion studies [48]. The impedance spectroscopy data are consistent with the corrosion currents calculated according to the polarization curves.

Several factors can explain the increase in the corrosion resistance. It is obvious that the addition of the nanodiamond particles plays a major role in the improved corrosion resistance and they act as an inert physical barrier to the initiation and development of the corrosion attack. In addition, there is a possibility of a large number of microcells formation in the nickel matrix. Nanodiamond particles will act as a cathode, and nickel as an anode [4]. Such corrosive galvanic

* Corresponding author
E-mail: Iryna.Makarava@lut.fi
DOI: 10.1016/j.surfcoat.2019.125063
Post-print of article published in journal Surface and coating technology (2019).

couples contribute to anodic polarization. Thus, Ni-nanodiamond coatings have better corrosion resistance [4].

The key role in another explanation belongs to the texture changing of the coating. It is well known that dense and packed crystal growth planes often dissolve faster due to the lower energy required for bond breaking and, therefore, active dissolution of atoms occurs in a certain direction [4]. In this work, the (111) planes were more closely packed compared to the (200) planes and probably contributed to an increase in the corrosion resistance of the studied composite coatings.

4. Conclusions

The electrochemical stage is the limiting stage of nickel ion reduction in the presence of nanodiamonds in the potential ranged from –0.4 to –0.8 V. The nanodiamonds addition into the Ni plating electrolyte led to an increase in the cathode polarization and accelerated the transition of nickel to a passive state. The presence of individual nanodiamonds was possibly indicated by the ImEFM measurements. The addition of nanodiamond particles allowed the formation of a fine crystalline nanocomposite coating with rougher surface topology and smaller crystalline sizes in comparison with pure nickel. Nanodiamond-containing coatings demonstrated an increase of the surface microhardness together with higher wear resistance with a decrease of the friction coefficient. These coatings demonstrated better corrosion resistance with a clear decrease in corrosion currents and a shift of the corrosion potential to more noble values. The charge transfer resistance (R_c) increased with the addition of nanodiamond particles, which is an indicator of the increased corrosion resistance. The increase of nanodiamond concentration in electrolyte from 10^{-3} to $5 \cdot 10^{-2}$ ($g \cdot dm^{-3}$) led to improved corrosion resistance and lower sliding friction.

5. Acknowledgements

This study was financially supported by the Governmental Research Program of Belarus (No. 20141326).

References

[1]. L. Wang, Y. Gao, Q. Xue, H. Liu, T. Xu, Effects of nano-diamond particles on the structure and tribological property of Ni-matrix nanocomposite coatings, Mater. Sci. Eng. A. 390 (2005) P. 313−318. https://doi.org/10.1016/j.msea.2004.08.033.

[2]. K. Strzelczak, Quality control of a metallic dental bur with a diamond coating, Production engineering archives. 19 (2018) 26−29. https://doi.org/10.30657/pea.2018.19.06.

* Corresponding author
E-mail: Iryna.Makarava@lut.fi

DOI: 10.1016/j.surfcoat.2019.125063
Post-print of article published in journal Surface and coating technology (2019).

[3] M. Adabi, A.A. Amadeh, Electrodeposition mechanism of Ni−Al composite coating, Trans. Nonferrous Met. Soc. China 24 (2014) 3189−3195. https://doi.org/10.1016/S1003-6326(14)63459-2.

[4] A. Hefnawy, N. Elkhoshkhany, A. Essam, Ni–TiN and Ni-Co-TiN composite coatings for corrosion protection: Fabrication and electrochemical characterization, J. Alloys Compd. 735 (2018) 600−606. https://doi.org/10.1016/j.jallcom.2017.11.169.

[5] S.-K. Kim, T.-S. Oh, Electrodeposition behavior and characteristics of Ni-carbon nanotube composite coatings, Trans. Nonferrous Met. Soc. 21 (2011) s.68−s.72. https://doi.org/10.1016/S1003-6326(11)61063-7.

[6] B. Pandeya, D. Das, A.K. Kar, Electrical and magnetic properties of electrodeposited nickel incorporated diamond-like carbon thin films, Appl. Surf. Sci. 337 (2015) 195–207. https://doi.org/10.1016/j.apsusc.2015.02.092.

[7] C. Wang, L. Shen, M. Qiu, Z. Tian, W. Jiang, Characterizations of Ni-CeO_2 nanocomposite coating by interlaced jet electrodeposition, J. Alloys Compd. 727 (2017) 269−277. https://doi.org/10.1016/j.jallcom.2017.08.105.

[8]. S. Ahmadiyeh, A. Rasooli, M.G. Hossein, Ni–B/SiC nanocomposite coating obtained by pulse plating and evaluation of its electrochemistry and mechanical properties, Surface Engineering https://doi.org/10.1080/02670844.2018.1498823.

[9] C. Liu, F. Su, J. Liang, Producing cobalt–graphene composite coating by pulse electrodeposition with excellent wear and corrosion resistance, Appl. Surf. Sci. 351 (2015) 889−896. https://doi.org/10.1016/j.apsusc.2015.06.018.

[10] M.Y. Rekha, S. Chandan, Microstructure and corrosion properties of zinc-graphene oxide composite coatings. Corrosion Science. Vol. 152, 15 2019, P. 234−248. https://doi.org/10.1016/j.corsci.2019.03.015.

[11] C.T.J. Low, R.G.A. Wills, F.C. Walsh, Electrodeposition of composite coatings containing nanoparticles in a metal deposit, Surf. Coat. Technol. 201 (2006) 371–383. https://doi.org/10.1016/j.surfcoat.2005.11.123.

[12] V.V. Yaskelchik, M.V. Anan'ev, T.N. Ostanina, I.M. Zharsky, A.A. Chernik, N.I. Ostanin, Sedimentation of ultradispesed diamonds in citrate electrolyte for electrodeposition of copper Izvestiya visshih uchebnih zavedenii. Poroshkovaya metallurgiya i funkcionalnie pokritiya. 2017 (4) 53−61. https://doi.org/10.17073/1997-308X-2017-4-53-61.

[13] M. Sheng, W. Weng, Y. Wang, Q. Wu, S. Hou, Co-W/CeO_2 composite coatings for highly active electrocatalysis of hydrogen evolution reaction, J. Alloys Compd. 743 (2018) 682−690. https://doi.org/10.1016/j.jallcom.2018.01.356.

* Corresponding author
E-mail: Iryna.Makarava@lut.fi
DOI: 10.1016/j.surfcoat.2019.125063
Post-print of article published in journal Surface and coating technology (2019).

[14] N. Elkhoshkhany, A. Hafnway, A. Khaled, Electrodeposition and corrosion behavior of nano-structured Ni-WC and Ni-CoWC composite coating, J. Alloys Compd. 695 (2017) 1505−1514. https://doi.org/10.1016/j.jallcom.2016.10.290.

[15] A. Laszczynska, J. Winiarski, B. Szczygieł, I. Szczygieł, Electrodeposition and characterization of Ni–Mo–ZrO_2 composite coatings, Appl. Surf. Sci. 369 (2016) 224−231. https://doi.org/10.1016/j.apsusc.2016.02.086.

[16] A.A. Kasach, I.I. Kurilo, D.S. Kharitonov, S.L. Radchenko, I.M. Zharskii, Effect of Sonochemical Treatment Modes on the Electrodeposition of Cu–Sn Alloy from Oxalic Acid Electrolyte, Russian Journal of Applied Chemistry, (2018) 91 (4) P. 591−596 doi: 10.1134/S1070427218040092.

[17] F. Wang, S. Arai, M. Endo, Preparation of nickel-carbon nanofiber composites by a pulse-reverse electrodeposition process, Electrochem. Commun. 7 (2005) 674−678. https://doi.org/10.1016/j.elecom.2005.04.016.

[18] B.-G. An, L.-X. Li, H.-X. Li, Electrodeposition in the Ni-plating bath containing multi-walled carbon nanotubes, Mater. Chem. Phys. 110 (2008) 481−485. https://doi.org/10.1016/j.matchemphys.2008.03.007.

[19] I.V. Antihovich, N.M. Ablazhey, A.A. Chernik, I.M. Zharsky, Electrodeposition of Nickel and Composite Nickel-Fullerenol Coatings from Low-Temperature Sulphate-Chloride-Isobutyrate Electrolyte, Procedia Chemistry. 10 (2014) 373–377. https://doi.org/10.1016/j.proche.2014.10.063.

[20] D. Liua, W. Zhao, S. Liu, Q. Cen, Q. Xue, Comparative tribological and corrosion resistance properties of epoxy composite coatings reinforced with functionalized fullerene C_{60} and graphene Surface and Coatings Technology, 286, 25 (2016) P. 354−364.

[21]. G. Sheela, M. Pushpavanam, Diamond-dispersed electroless nickel coatings, Metal Finishing, 100, 1 (2002) 45−47. https://doi.org/10.1016/S0026-0576(02)80018-6.

[22]. M. Wang, R.-C. Wang, C. Peng, Y. Feng, C. Zhang, L. Deng, Preparation of Ni-diamond composite coating by composite electroplating, Journal of Central South University (Science and Technology), 44 (7) (2013) P. 2688−2695.

[23]. H. Ogihara, A. Hara, K. Miyamoto, N. K. Shrestha, T. Kaneda, S. Ito, T. Saji, Synthesis of super hard Ni–B/diamond composite coatings by wet processes, Chem. Commun., 46 (2010) 442−444. https://doi.org/10.1039/B914242H

[24]. T. Tsubota, Sh. Tanii, T. Ishida, M. Nagata, Y. Matsumoto, Composite electroplating of Ni and surface-modified diamond particles with silane coupling regent, Diam. Relat. Mater. 14 (2005) 608−612. https://doi.org/10.1016/j.diamond.2005.01.013.

* Corresponding author
E-mail: Iryna.Makarava@lut.fi

DOI: 10.1016/j.surfcoat.2019.125063
Post-print of article published in journal Surface and coating technology (2019).

[25]. I.V. Antsikhovich, A.A. Chernik, I.M. Zharsky, Properties of composite nickel coatings obtained from low-temperature tartaric electrolytes, Galvanotechnika I obrabotka poverhnosti. 23, 2 (2015) 38–43. https://doi.org/10.1016/j.proche.2014.10.063.

[26]. G.K. Burkat, T. Fujimura, V.Yu. Dolmatov, E.A. Orlova, M.V. Veretennikova, Preparation of composite electrochemical nickel-diamond and iron-diamond coatings in the presence of detonation synthesis nanodiamonds Diam. Relat. Mater. 14 (2005) 1761−1764. https://doi.org/10.1016/j.diamond.2005.08.004.

[27]. L. Wang, Y. Gao, Q. Xue, H. Liu, T. Xu, Effects of nano-diamond particles on the structure and tribological property of Ni-matrix nanocomposite coatings, Mater. Sci. Eng. A , 390 (2005). 313−318. https://doi.org/10.1016/j.msea.2004.08.033.

[28]. L. Wang, Y. Gao, H. Liu, Q. Xue, T. Xu, Effects of bivalent Co ion the co-deposition of nickel and nano-diamond particles, Surf. Coat. Technol., 191 (2005) 1−6. https://doi.org/10.1016/j.surfcoat.2004.03.047.

[29]. S. You, M. Mases, I. Dobryden, A.A. Green, M.C. Hersam, A.V. Soldatov, Probing structural stability of double-walled carbon nanotubes at high non-hydrostatic pressure by Raman spectroscopy, High pressure res. 31, 1 (2011) 186–190. https://doi.org/10.1080/08957959.2011.562897.

[30] T. Xu, K. Xu, J. Zhao. TEM and HREM studies on ultradispersed diamonds containing soot formed by explosive detonation, Mater. Sci. Eng. B. 38, 1–2 (1996) L1−L4. https://doi.org/10.1016/0921-5107(95)01526-4.

[31] V. Yu. Dolmatov Detonation synthesis ultradispersed diamonds: Properties and applications Russian Chemical Reviews. 70, 7 (2001) 607−626. https://doi.org/10.1070/RC2001v070n07ABEH000665.

[32] L. Jinlong, L. Tonxiang, W. Chen. Effect of electrodeposition temperature on grain orientation and corrosion resistance of nanocrystalline pure nickel, J. Solid State Chem. 240 (2016) 109–114. https://doi.org/10.1016/j.jssc.2016.05.025.

[33] F. Nasirpouri, M.R. Sanaeian, A.S. Samardak, E.V. Sukovatitsina, A.V. Ognev, L.A. Chebotkevich, M.-G. Hosseini, M. Abdolmaleki. An investigation on the effect of surface morphology and crystalline texture on corrosion behavior, structural and magnetic properties of electrodeposited nanocrystalline nickel films, Appl. Surf. Sci. 276 (2013) 604–608. https://doi.org/10.1016/j.apsusc.2013.12.053.

[34] N.P. Wasekar, P. Haridoss, S.K. Seshadri, G. Sundararajan, Influence of mode of electrodeposition, current density and saccharin on the microstructure and hardness of

* Corresponding author
E-mail: Iryna.Makarava@lut.fi
DOI: 10.1016/j.surfcoat.2019.125063
Post-print of article published in journal Surface and coating technology (2019).

electrodeposited nanocrystalline nickel coatings, Surf. Coat. Technol. 291 (2016) 130–140. https://doi.org/10.1016/j.surfcoat.2016.02.024.

[35] H. Alimadadi, A.B. Fanta, T. Kasama, M.A.J. Somers, K. Pantleon, Texture and microstructure evolution in nickel electrodeposited from an additive-free Watts electrolyte, Surf. Coat. Technol. 299 (2016) 1−6. https://doi.org/10.1016/j.surfcoat.2016.04.068.

[36] B. Lv, Z. Hu, X. Wang, B. Xu, Electrodeposition of nanocrystalline nickel assisted by flexible friction from an additive-free Watts bath, Surf. Coat. Technol. 270 (2015) 123–131. https://doi.org/10.1016/j.surfcoat.2015.03.012.

[37] I.V. Makarova, D.S. Kharitonov, I.B. Dobryden, A.A. Chernik, Corrosion behavior in acid and alkaline media of nickel coatings deposited at room temperature, Russ. J. Appl. Chem. 91 (2018) 1441–1450. https://doi.org/ 10.1134/S1070427218090069.

[38] I.V. Antsikhovich, D.S. Kharitonov, A.A. Chernik, I.B. Dobryden, Corrosion resistance of nickel coatings deposited from low-temperature nickel-plating electrolytes, Russ. J. Appl. Chem. 90 (2017) 566–573. https://doi.org/10.1134/S1070427217040127.

[39] D. Platz, E.A. Tholén, D. Pesen, D.B. Haviland, Intermodulation atomic force microscopy Appl. Phys. Lett. 92, 153106 (2008); https://doi.org/10.1063/1.2909569

[40] R. Borgani, D. Forchheimer, J. Bergqvist, P.-A. Thorén, O. Inganäs, D.B. Haviland, Intermodulation electrostatic force microscopy for imaging surface photo-voltage, Appl. Phys. Lett. 105 (2014) 143113; https://doi.org/10.1063/1.4897966.

[41] D. Nečas, P. Klapete, Gwyddion: an open-source software for SPM data analysis, Cent. Eur. J. Phys. 10,1 (2012) 181−188; https://doi.org/10.2478/s11534-011-0096-2.

[42] S. Mrowec, Z. Grzesik, Oxidation of nickel and transport properties of nickel oxide, J. Phys. Chem. Solids. 65 (2004) 1651–1657. https://doi.org/10.1016/j.jpcs.2004.03.011.

[43] M.A.M. Ibrahim, R.M. Al Radadi, Role of glycine as a complexing agent in nickel electrodeposition from acidic sulphate bath, Int. J. Electrochem. Sci., 10 (2015) 4946 – 4971

[44] T.D. Khokhlova, G.R. Yunusova, S.N. Lanin, Adsorption of Dyes in Studying the Surface Chemistry of Ultradispersed Diamond, Russian Journal of Physical Chemistry A, 92, 5 (2018) 1006–1010. https://doi.org/10.1134/S0036024418050175.

[45] Y.H. Ahmad, J. Tientong, M. Nar, N. D'Souza, A.M.A. Mohamed, T.D. Golden. Characterization and corrosion resistance of electrodeposited Ni–Mo–silicate platelet nanocomposite coatings, Surf. Coat. Technol. 259 (2014) 517–525. http://dx.doi.org/10.1016/j.surfcoat.2014.10.036.

* Corresponding author
E-mail: Iryna.Makarava@lut.fi
DOI: 10.1016/j.surfcoat.2019.125063
Post-print of article published in journal Surface and coating technology (2019).

[46] W. Huang, Y. Zhao, X. Wang, Preparing a high-particle-content Ni/diamond composite coating with strong abrasive ability, Surf. Coat. Technol. 235 (2013) 489–494. https://doi.org/10.1016/j.surfcoat.2013.08.008.

[47] X. Xi et al. Effect of phosphorus content on the properties of Ni-P coated diamond, Surf. Coat. Technol. 297 (2016) 27–33. https://doi.org/10.1016/j.surfcoat.2016.04.041.

[48] B. Wang, Y. Ma, C. Ran, G. Liu, Z. Hou, Preparation and Properties of Ni-W-rGO Composite Coatings Int. J. Electrochem. Sci. 14 (2019) 1884–1896, doi: 10.20964/2019.02.09

* Corresponding author
E-mail: Iryna.Makarava@lut.fi
DOI: 10.1016/j.surfcoat.2019.125063
Post-print of article published in journal Surface and coating technology (2019).

Highlights

1. Ni-nanodiamond coatings were electrodeposited from nickel-plating electrolyte at ambient temperature.
2. The composite coatings had a higher hardness, a higher wear resistance and roughness, lower friction coefficient than pure nickel coatings.
3. Nanodiamonds improved the corrosion resistance of composite coating.

* Corresponding author
E-mail: Iryna.Makarava@lut.fi
DOI: 10.1016/j.surfcoat.2019.125063
Post-print of article published in journal Surface and coating technology (2019).

Supplementary

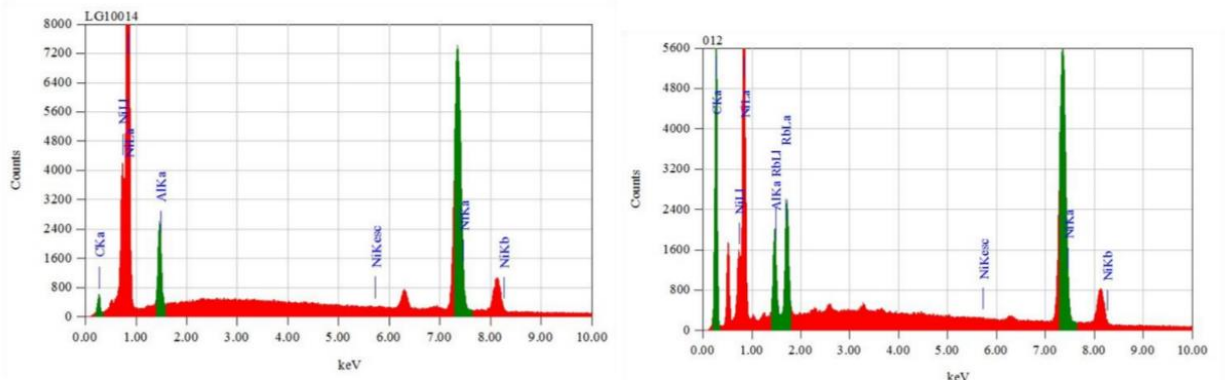

(*a*) (*b*)

Fig 1S. EDS plots of nickel (*a*) and nickel- nanodiamond (*b*) coatings

* Corresponding author
E-mail: Iryna.Makarava@lut.fi
DOI: 10.1016/j.surfcoat.2019.125063
Post-print of article published in journal Surface and coating technology (2019).